INTERNATIONAL JOURNAL FOR NUMERICAL METHODS IN FLUIDS
Int. J. Numer. Meth. Fluids **29**: 877–895 (1999)

A THREE-DIMENSIONAL HYBRID FINITE ELEMENT–VOLUME TRACKING MODEL FOR MOULD FILLING IN CASTING PROCESSES

D.M. GAO*

Industrial Materials Institute, National Research Council of Canada, 75 de Mortagne, Boucherville, Quebec J4B 6Y4, Canada

SUMMARY

Metal casting is a complicated process in which flow momentum plays a crucial role in the mould filling process due to the high velocity of the liquid metal. Inertia and gravity effects may cause splashing, jetting or undesirable filling of the metal flow into the mould cavity. When considering complex parts, the accurate prediction of mould filling behaviour using empirical knowledge and intuition is nearly impossible. Therefore, numerical modelling and simulation are essential to predict such a complex physical problem and assist in part with mould design. A mould filling analysis can help the mould designer to determine the size and location of the gate as well as a proper runner system design for ensuring a complete and balanced filling of the part. Such an analysis can also be used to predict potential product defects, such as air entrapment, porosities, and help in correct positioning of overflows and venting systems. A three-dimensional finite element model combined with a volume tracking method has been developed in this work to simulate the cavity filling for casting processes. A mixed formulation based on a four node tetrahedral element with a bubble function at the centroid ($P1^+/P1$) is employed to solve the flow equations. Such a finite element provides a small dimension of the element matrices and satisfies the Brezzi–Babuska condition to ensure a stable solution of the Navier–Stokes equations. A slip boundary condition combined with a friction model is implemented to better simulate the metal flow near the mould walls. An algebraic model is used to account for the turbulence effects during the mould filling. The flow fronts are tracked by a volume tracking method developed for the tetrahedral elements. This method can handle complicated flow front shapes and complex situations like merging and separation of flow fronts. The combination of a volume tracking technique with a FEM flow solver in three-dimensional unstructured meshes constitutes the major feature of this model. Examples of the filling simulations are presented to illustrate the capabilities of the numerical model. Copyright © 1999 John Wiley & Sons, Ltd.

KEY WORDS: mould filling; three-dimensional flow; finite element; mixed formulation; front tracking; volume tracking

1. INTRODUCTION

Metal casting is a complicated process that involves the high speed flow of a liquid metal filling into three-dimensional complex geometries. The metal flow during filling behaves in a very complex manner with phenomena such as frequent vortex formation, flow front merging and breaking, etc. The flow fronts directly affected by a such complex flow behaviour have

* Correspondence to: Process Modelling and Optimisation Section, Industrial Materials Institute, National Research Council of Canada, 75 de Mortagne, Boucherville, Quebec J4B 6Y4, Canada.

CCC 0271–2091/99/070877–24$17.50

generally very distorted shapes. Furthermore, the flow may simultaneously be subject to abrupt changes in direction and dimensions, which often result in the formation of undesirable isolated air pockets (also referred to as air entrapment) and consequently casting defects. When considering complex parts, the accurate prediction of mould filling behaviour using empirical knowledge and intuition is nearly impossible. Therefore, numerical modelling and simulation become an attractive approach to determine accurately the flow front shapes and locations, as well as the flow characteristics during the entire filling process.

The numerical tools for simulating casting processes have been increasingly employed in the casting industry in order to understand and improve casting techniques. The numerical simulations allow the designer to analyse and visualise the complete casting process from the metal injection to the final product. The detailed information on the flow, heat transfer and residual stress behaviour can be used to evaluate the feasibility of the mould/part design and help the optimisation of the operating conditions.

As far as the modelling of the mould filing is concerned, the precise tracking of the flow fronts of arbitrary shape and a robust algorithm of highly non-linear flow with moving interfaces are the major challenges [1]. In the case of the casting process, it becomes even more critical because the high speed flow is often associated with the appearance of the turbulence phenomenon and the geometrical complexity of the part. In addition, the coupling between a high speed viscous flow and the dynamic change of moving interface locations often leads to unstable solutions. Therefore, a numerical model that combines an accurate flow front tracking method and a robust flow solution is essential in order to obtain a true prediction of the filling behaviour. Since the mould filling can be considered as a moving interface problem, no distinction is made between the 'flow front' and the 'moving interface' in the following discussion.

Over the past 20 years, researchers have put a lot of effort into developing various numerical models to simulate the filling processes, including the heat transfer behaviour. The majority of these models are constructed based on the fixed mesh concept within the finite element or finite difference frameworks [2–12]. Hirt *et al.* [13] first introduced the volume of fluid (VOF) method to simulate the moving interface problems. This method has been applied increasingly to mould filling problems, mainly with the finite difference method [6,8,10,11]. The VOF method is considered the most significant and most referred to work among the front tracking methods in engineering applications. It is classified as one of the three pioneer volume tracking methods [14]. The basic idea of the VOF method and other volume tracking methods is to evaluate the fluid quantity flowing in/exiting from each element to obtain a new fluid volume fraction field, and consequently the moving interface positions. A reconstruction of the moving interface is necessary to ensure an accurate calculation of the fluid quantity flowing across the faces of the interface elements that contain the moving interfaces. The reconstruction of the moving interface by the VOF method has been improved in many aspects [14–16]. Rider *et al.* [14] extended this method to unstructured meshes in two and three dimensions. Recently, it has been used in the finite element framework to solve two-dimensional free-surface and moving boundary problems [17]. For casting applications, the volume tracking methods have been proven to be capable of tracking the flow front of arbitrary shapes for complex problems involving front distortion, breaking, etc. Another interesting alternative for tracking the moving interfaces is referred to as pseudo-concentration equation approach, often used with the finite element method. In 1987, Thompson first introduced this idea for creeping flows with interfaces [18]. The approach consists of using a pseudo-concentration function defined in the entire cavity domain and solving directly a hyperbolic equation to determine the moving interface movement. A smoothing technique was implemented to transform the concentration

function into a continuous function. The moving interface is represented by a specific value of the pseudo-concentration function. The flow solution in the empty area (or air) is needed to obtain a correct solution of the hyperbolic equation. Large differences of the material properties, such as density and viscosity between the liquid and the air, have to be dealt with when solving the flow equations. This approach has been adapted and improved by other researchers [3,4,7,19] to simulate the mould filling problems for casting and plastics injection processes.

Since the primary target in this research is die casting, which generally involves the filling of the thin wall cavities, it is felt necessary to summarise some of the more significant works on this subject. Compared with the thick castings, little work has been performed in the field of thin wall cavity filling analysis. The main reason is that these kind of parts have generally complex geometries, such as transmission housing, engine covers, etc., in which the part thickness is much smaller than the global dimensions. The conventional numerical discretisation results in a highly distorted mesh, which often causes numerical instabilities. Some recent work has used a shell element approach similar to those used in polymer injection moulding [20]. Zhang *et al*. [12] used a potential flow theory and took the pressure as a primary variable to model the flow behaviour in thin wall castings. They assumed that the flow is invicid and irrotational. Using the shell element idea, other works [2,21–23] formulated the two-dimensional Navier–Stokes equations in local elements, then transformed them into a global co-ordinate system. Results have been obtained for relatively simple geometries using these models. However, such simplified models will fail to predict the flow behaviour in the parts having large curvature and complex geometries, therefore the validity of the velocity transformation still needs to be proved.

A three-dimensional finite element model is favoured in this work in order to predict the flow behaviour for cavity filling of complex shapes, including thin wall cavity filling. Several reasons have motivated this choice. Among them are (1) the theory for the two-dimensional shell approach is applicable only for highly viscous flow, which is no longer valid for casting processes; (2) parts have more and more complex geometry and many of them have thin and thick sections simultaneously, therefore three-dimensional models are more suitable and can be applied to parts of arbitrary shapes; (3) from the mesh point of view, the shell mesh is not trivial for complex parts, while the three-dimensional one is much more straightforward.

The three-dimensional model developed in the current work is initially built to simulate the thin wall casting filing. However, it can be applied to thick parts as well. The main features of the model are: (1) mixed finite element formulation solving the Navier–Stokes equations for transient incompressible viscous flow; (2) volume tracking technique developed in three-dimensional unstructured meshes for capturing the flow front position during filling.

2. MATHEMATICAL MODELS

As discussed in the previous section, there are generally two categories of numerical models to treat the discontinuity due to the presence of interface between the liquid metal and the air (flow fronts) using the fixed mesh concept. The first associates the flow front position to a specific value of a pseudo-concentration function defined in the entire domain including air, and the flow front can be captured by solving the hyperbolic transport equation. A flow solution in the entire domain including air or a portion of areas occupied by air needs to be performed [3,4,7,18,19]. This approach implies that the flow solver has to deal with the discontinuity of the material properties across the interface. The second approach solves the

flow equations only in the filled region and the flow front location is determined by the volume tracking method, which consists of evaluating the flow rate entering and exiting each element across or connecting to the flow front [5,13,14]. A filling factor is defined to represent the filling state of each element.

The second approach is adopted in the present study, and only the filled region is considered for solving the flow equations. This eliminates the numerical difficulties generated by the discontinuity of the material properties across the moving interface when solving the flow equations.

2.1. Flow equations

The momentum and mass conservation of a Newtonian fluid flow are described by the Navier–Stokes equations:

$$\rho\left(\frac{\partial \mathbf{u}}{\partial t} + \mathbf{u}\cdot\nabla\mathbf{u}\right) = -\nabla p + \nabla\cdot[\mu(\nabla\mathbf{u} + \nabla\mathbf{u}^T)] + \rho\mathbf{g} \quad \text{on } \Omega, \tag{1}$$

$$\nabla\cdot\mathbf{u} = 0 \quad \text{on } \Omega, \tag{2}$$

where t, ρ, $\mathbf{u}$, p, μ denote the time, density, velocity vector, pressure and viscosity respectively, and $\rho\mathbf{g}$ is the gravity force.

2.2. Boundary conditions

As in any differential equations, the solution of the Navier–Stokes equations requires the appropriate boundary conditions specified on the boundary of the flow domain. Figure 1 shows a two-dimensional scheme illustrating the various boundaries involved in a filling process.

Typically, the following boundary conditions are imposed:

(a) At the inlet where the flow enters into the cavity, the velocity vector is imposed,

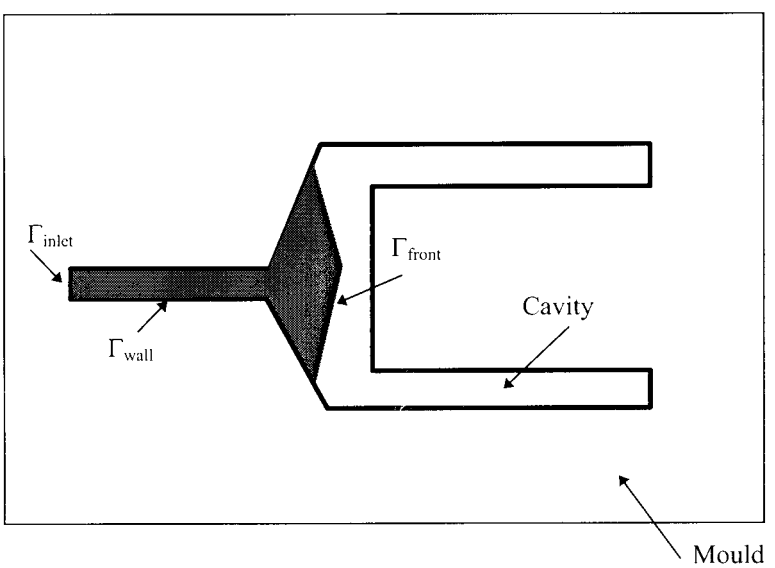

Figure 1. Two-dimensional schematic of a mould cavity.

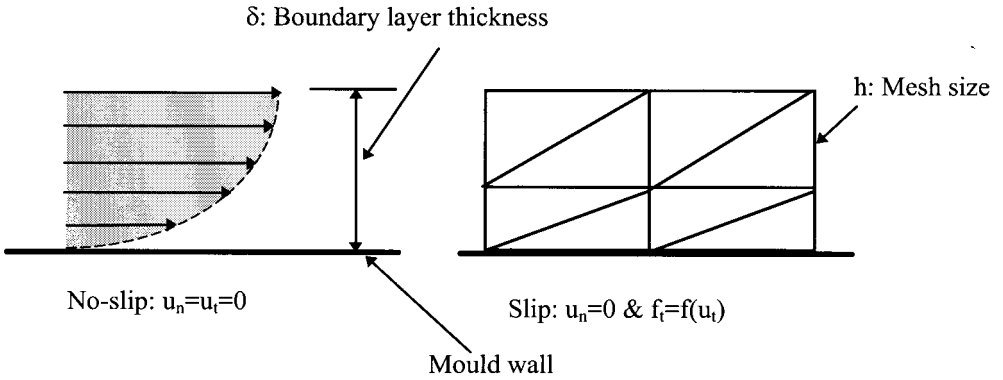

Figure 2. Illustration of the friction model.

$$\mathbf{u} = \bar{\mathbf{u}} \quad \text{on } \Gamma_{\text{inlet}}. \tag{3}$$

(b) At the moving front, the surface tension is neglected and the normal surface stress boundary condition is expressed as:

$$f_{\text{n}} = -p + 2\mu\left(\frac{\partial u_{\text{n}}}{\partial n}\right) = p_0 \quad \text{on } \Gamma_{\text{front}}, \tag{4}$$

where f_{n} is the normal stress, p is the pressure on the flow front surface, p_0 is the atmosphere pressure and u_{n} is the normal velocity at the front.

Since the flow in castings has a very high Reynolds number, it is reasonable to assume that the viscous term in the surface stress condition is negligible. This reduces the surface stress condition to a simple Dirichlet-type condition on pressure,

$$p = p_0. \tag{5}$$

It should be noted that the situation may become more complicated if the venting of the mould is not adequate or if the air is trapped in the cavity. In such a case, the air pressure increases with time and the flow properties of air play an important role in determining the pressure required for the filling as well as the position of the flow front. The perfect venting condition is assumed for the simulations presented. This means that the air can escape from the mould wall without resistance.

(c) On the mould wall, velocity boundary conditions are considered as either no-slip, where $\mathbf{u} = 0$ at the wall, or slip with or without friction, where the normal velocity $u_{\text{n}} = \mathbf{u}\cdot\mathbf{n} = 0$. The friction f_{t}, can be evaluated as a function of the tangent velocity u_{t} at the wall,

$$f_{\text{t}} = f(u_{\text{t}}) \quad \text{on } \Gamma_{\text{wall}}. \tag{6}$$

The function f is dependent on the flow regime and the ratio between the mesh size and the boundary layer thickness (see Figure 2). If the thickness of the boundary layer is much smaller (more than one order of magnitude) than the mesh size, a free-slip condition is used. If the mesh size is about the same order as the boundary layer, a partial-slip condition with friction is applied. Ideally, one should mesh from the mould wall, refining the boundary layer to capture the large variation of the velocity fields in such a layer. Unfortunately, with current computer powers, it is almost impossible to mesh the boundary layer fine enough to model the high gradient of the velocity field near the mould wall.

To make a proper choice about the type of slip boundary conditions, one has to evaluate the boundary layer thickness. Examples can be found in classical handbooks for simplified situations. For example, if we approximate the boundary layer in castings by a fluid passing around a simple flat plate parallel to the flow, the thickness of such a boundary layer can be evaluated by the following expression [24]:

$$\delta \approx 5\sqrt{\frac{vL}{u}}, \tag{7}$$

where v, L and u represent kinematic viscosity, plate length and velocity magnitude respectively. If the plate is 10 cm long, the velocity is 10 $\mathrm{m\,s^{-1}}$ and the kinematic viscosity is 1.0×10^{-5} $\mathrm{m^2\,s^{-1}}$, the boundary layer thickness is 1.58 mm. This is the typical size of the mesh used in filling simulations. Therefore, in most cases a slip boundary condition with friction is imposed to mimic the boundary layer effects.

In practice, the friction is found to be extremely sensitive and very difficult to evaluate for most filling analysis, particularly for the gravity casting process where the filing velocity is directly determined by the ratio of the gravity force and the friction of the mould walls. Furthermore, the friction affects the flow front movement near the mould walls. Since the present paper is limited to presenting the main features of a three-dimensional filling model, no details are given here concerning the sensitivity of the friction. The effects of the friction on mould filling will be investigated in a separate paper. In this work, the function f is assumed to be proportional to the quantity $|u_t|u_t$:

$$f_t = f(u_t) = -C|u_t|u_t, \tag{8}$$

where C is the friction coefficient.

2.3. Turbulence model

Since the flow encountered in casting filling is typically turbulent, a proper choice of the turbulent model is needed to ensure a reasonable prediction of the turbulence effects.

Considering the available computer power and the complexity of the industrial parts, this study is mainly interested in zero equation models, i.e. algebraic models. Currently, the Smagorinsky model [25–27] is implemented to evaluate the eddy viscosity according to

$$\mu_t = \alpha h^2 |\nabla \mathbf{u} + \nabla \mathbf{u}^T|, \quad \alpha = 0.01, \tag{9}$$

where μ_t is the eddy viscosity and h is the size of the elements.

3. NUMERICAL MODELS

The numerical model developed in this work comprises two numerical methods having the distinct nature and theoretical background. The finite element method is utilised for flow modelling, while the volume tracking method is developed for flow front tracking. Both methods are described in the following sections, as well as their coupling procedure.

3.1. Flow modelling

3.1.1. The variational form. The variational form is the starting point for building a finite element discretisation of any PDE system. A Galerkin-type weighting function is used here for constructing the variational form denoted w. The weighting functions for the velocity vector

and pressure scalar are denoted as υ and q respectively, and the final weak form after the integration by parts can be written as:

$$w = \int_\Omega \left(\rho \frac{\partial \mathbf{u}}{\partial t} + \rho \mathbf{u} \cdot \nabla \mathbf{u} - \rho \mathbf{g} \right) \upsilon \, \mathrm{d}\Omega + \int_\Omega [\mu(\nabla \mathbf{u} + \nabla \mathbf{u}^T) : (\nabla \upsilon + \nabla \upsilon^T)] \, \mathrm{d}\Omega - \int_\Omega p \nabla \cdot \upsilon \, \mathrm{d}\Omega + \int_\Omega \nabla \cdot \mathbf{u} q \, \mathrm{d}\Omega - \int_{\partial\Omega} (\upsilon_t f_t) \, \mathrm{d}\Gamma_w - \int_{\partial\Omega} (\upsilon_n f_n) \, \mathrm{d}\Gamma_f, \quad \forall \upsilon, q, \tag{10}$$

where

$$f_t = \mu \left(\frac{\partial u_t}{\partial n} + \frac{\partial u_n}{\partial t} \right), \qquad f_n = -p + 2\mu \frac{\partial u_n}{\partial n},$$

and υ_t, υ_n denote the tangent and normal components of υ respectively, and Γ_f and Γ_w represent the moving flow front and the mould wall boundaries. The friction conditions f_t on the mould walls as well as the normal stress condition f_n are discussed in the previous sections.

3.1.2. Finite element implementation. A mixed finite element formulation based on a four node tetrahedral $P1^+/P1$ elements [28–30] has been implemented in this work (see Figure 3).

This element, having a fifth node in its centroid, satisfies the Brezzi–Babuska conditions, which are necessary to ensure a stable solution for the Navier–Stokes equations using the classical Galerkin method. In addition, it represents several important advantages: (1) the four node element provides a minimum dimension of the element matrix compared with other three-dimensional finite elements; and (2) tetrahedral elements have a great ability to represent the complex geometries. Since the element is linear, the mesh refinement algorithm can be easily implemented in the future.

For a given element, a fifth node at the centroid is considered to construct the piecewise linear approximation ($P1^+$) for the velocity field. This decomposes the element into four

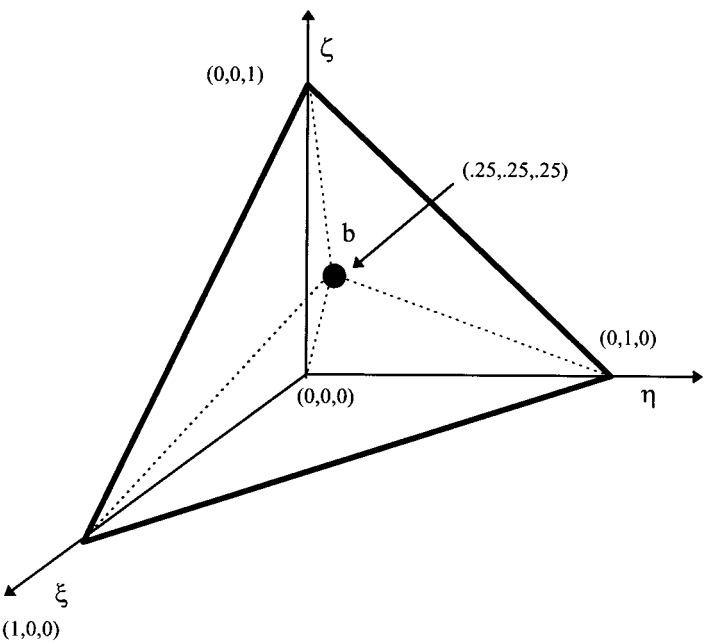

Figure 3. Four node $P1^+/P1$ element.

subtetrahedrons. The trial function for velocity is constituted by four linear components and a bubble function. The pressure is defined linearly using the four vertices. In this work, a bubble function being zero at the element boundary and piecewise-linear on subtetrahedrons was chosen for the sake of the numerical integration.

$$\mathbf{u} = \sum_{i=1}^{4} N_i \cdot \mathbf{u}_i + N_\mathrm{b} \cdot \mathbf{u}_\mathrm{b}, \quad N_\mathrm{b} = 4 \cdot \mathrm{Min}(N_1, \ldots, N_4), \tag{11}$$

$$p = \sum_{i=1}^{4} N_i \cdot p_i, \tag{12}$$

where $\mathbf{u}_i$ and $\mathbf{u}_\mathrm{b}$ are velocity vectors at the vertices and the centroid respectively, P_i is pressure at the vertices, N_i is the component of the linear trial functions and N_b is the bubble function.

Even though the centroid is used as a part of the velocity field approximation when building the elementary matrices, it then can be eliminated by the 'static condensation' procedure [29] at element level, leading to the initial four node tetrahedrons.

The finite element discretisation of the flow equations leads to a highly non-linear system. The Newton–Raphson method is implemented to linearise the equations.

The classic first-order Euler implicit scheme has been used to evaluate the transient terms, which are

$$\left(\frac{\partial \mathbf{v}}{\partial t}\right)^{n+1} = \frac{\mathbf{v}^{n+1} - \mathbf{v}^n}{\Delta t}. \tag{13}$$

The matrix form of the algebraic system resulted from the discretisation can be expressed as:

$$[M]\frac{\{\mathbf{v}^{n+1} - \mathbf{v}^n\}}{\Delta t} + [K]\{\mathbf{v}^{n+1}\} = \{F^{n+1}\}, \tag{14}$$

where $\mathbf{v}$ represents an unknown vector, including the velocity components and pressure field $\{u, v, w, p\}$, F is a source term that involves gravity or any other body forces. $[M]$ and $[K]$ are the mass and tangent matrices respectively. Subscripts n and $n+1$ denote the previous and current time steps respectively.

3.2. The volume tracking method

For a general filling problem, the flow front motion, as a moving interface, can be represented by a volume fraction function $f(\mathbf{x}, t)$ defined in the entire calculation domain (also called pseudo-concentration function, see [18]). The value of the f function is unity for the filled area and zero elsewhere. Therefore, the discontinuity in the $f(\mathbf{x}, t)$ function represents moving interface locations. The motion of the moving interface transported by a velocity field $(\mathbf{u})$ is governed by

$$\frac{\mathrm{D}f(\mathbf{x}, t)}{\mathrm{D}t} = \frac{\partial f}{\partial t} + \mathbf{u} \cdot \nabla f = 0, \tag{15}$$

where $\mathrm{D}f/\mathrm{D}t$ is the material derivative and $f(\mathbf{x}, t)$ is Lagragian invariant. Equation (15) governs the movement of an interface and constitutes the basis of all front tracking techniques.

Moving interfaces are obtained by ensuring the discontinuity of the function f. This requires a special numerical treatment because none of the classical numerical methods are suitable for solving a scalar function with singularities. Two types of approaches can be found in the literature. The first solves Equation (15) directly by various numerical techniques, such as the Lesaint–Raviart [19], or smoothing the f function [3,18]. The second approach transforms

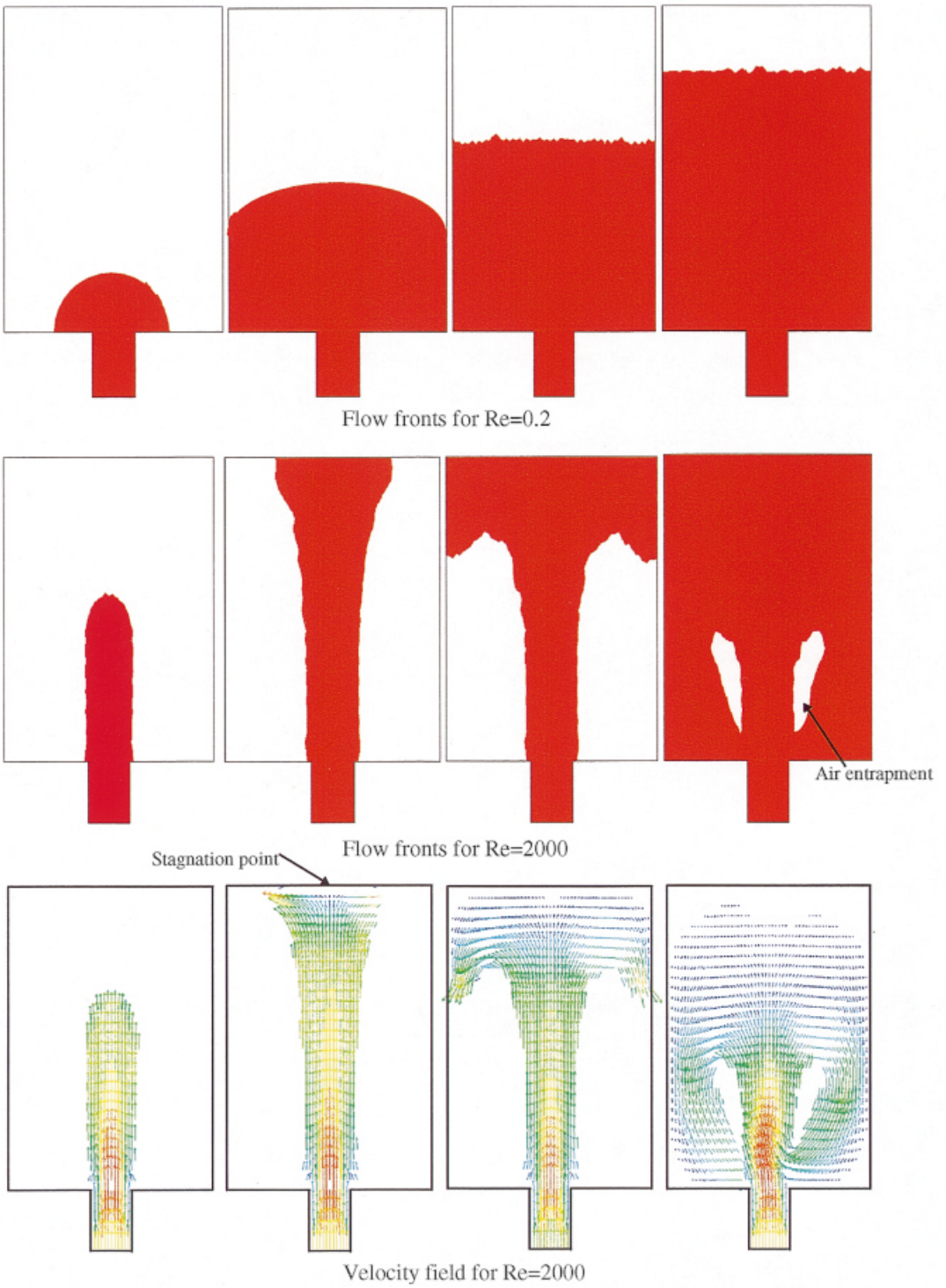

Plate 1. Flow front positions and velocity fields for filling a rectangular plate.

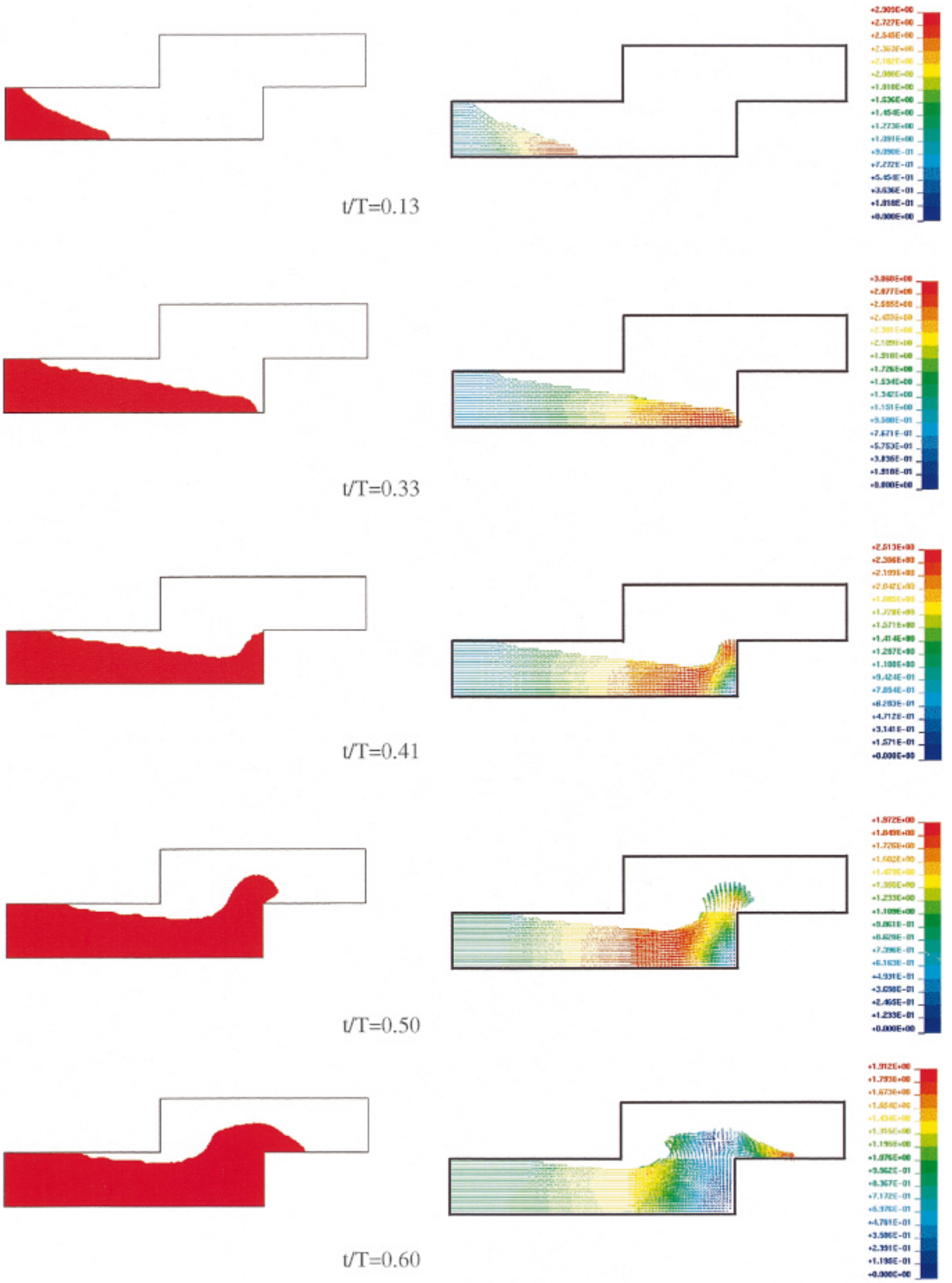

Plate 2. Flow front positions and corresponding velocity vectors for a step cavity filling.

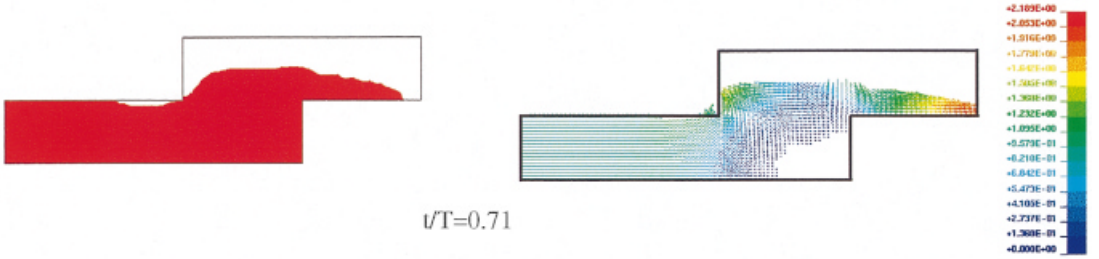

t/T=0.71

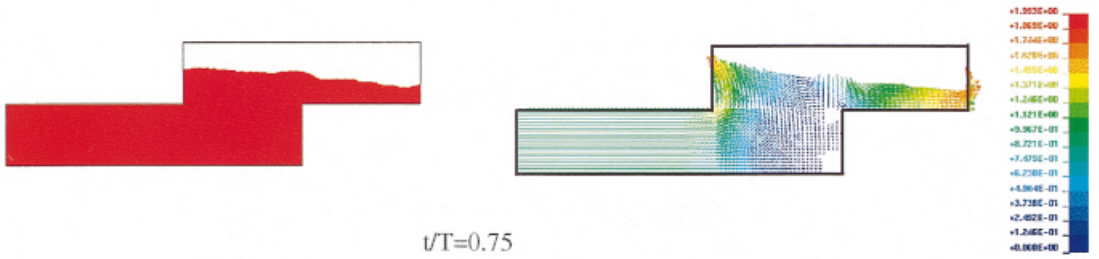

t/T=0.75

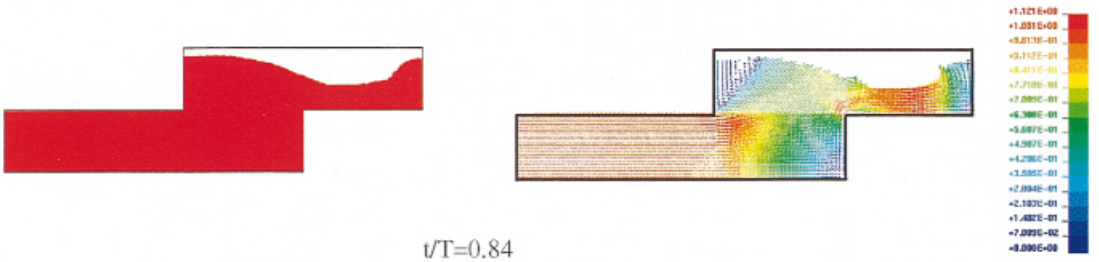

t/T=0.84

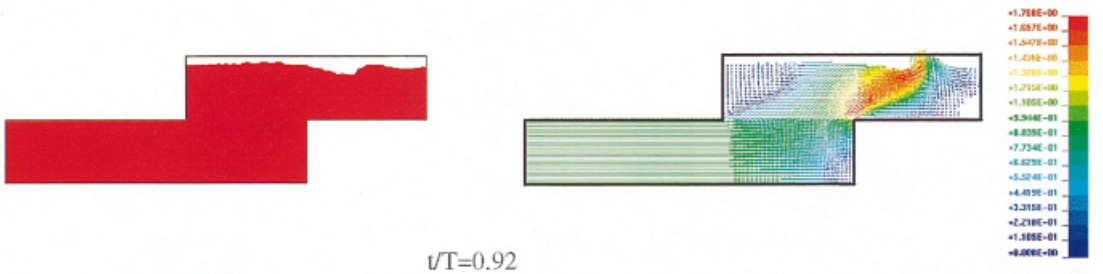

t/T=0.92

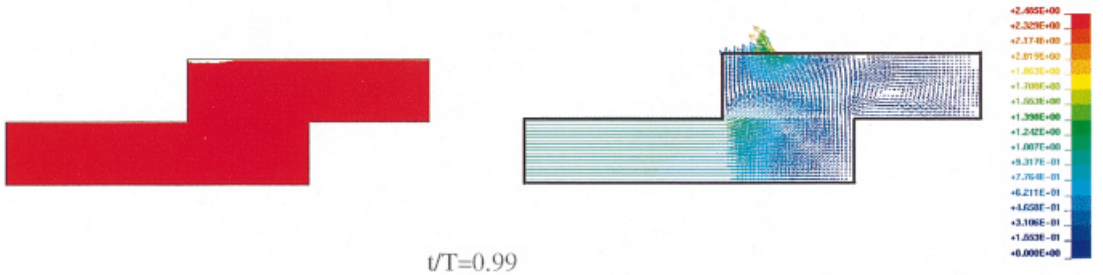

t/T=0.99

Plate 2 (*Continued*)

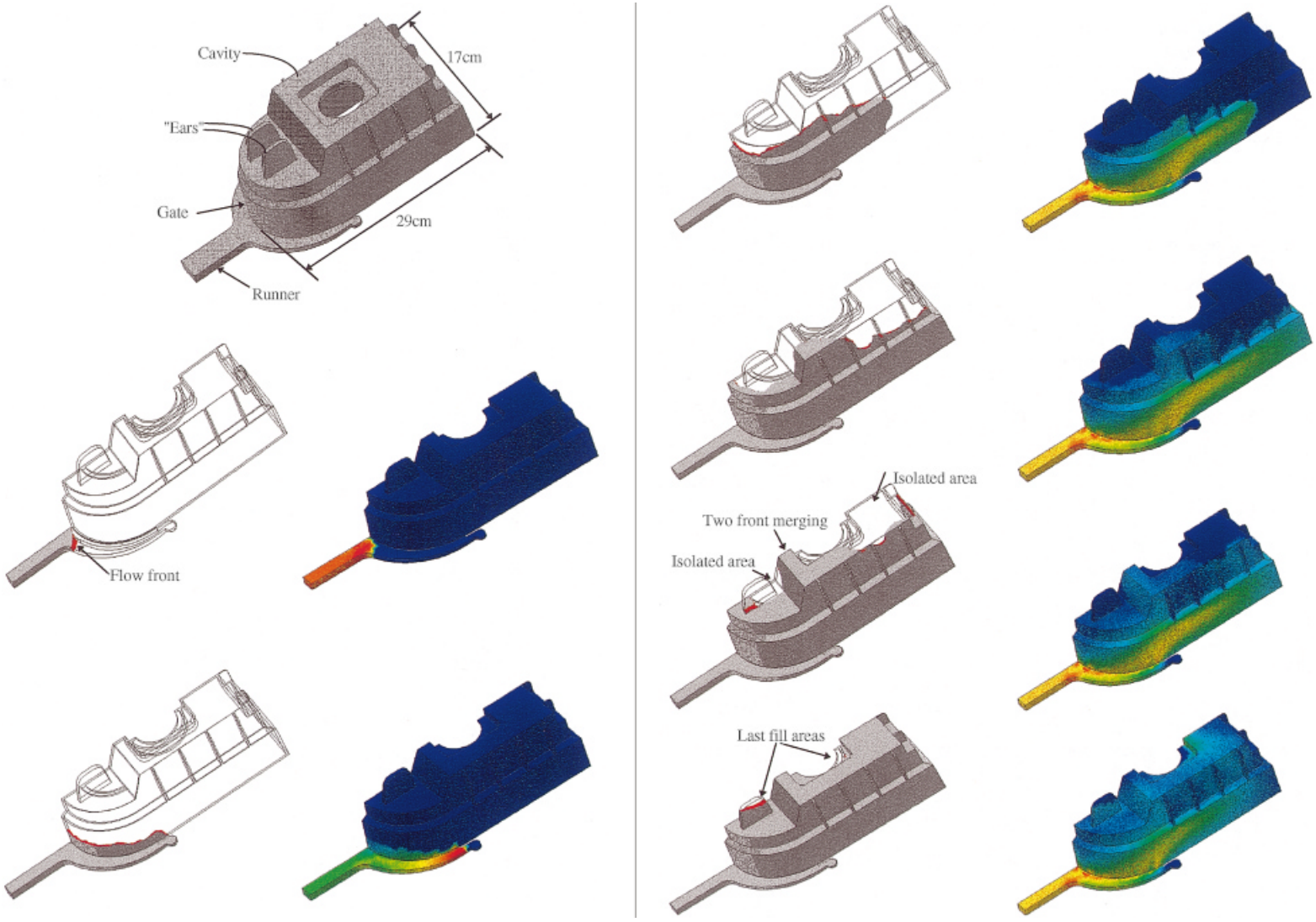

Plate 3. Flow front positions and velocity magnitudes of a die casting part.

Plate 4. Flow front positions and velocity magnitudes of a connector housing.

Equation (15) into a control volume concept and solves the hyperbolic equation by evaluating flow quantity of control volumes [14]. All volume tracking methods can be derived from the latter approach. In the present study, a volume tracking method is developed to track the flow front movement.

Even though the volume tracking method has been widely used and applied for various academic and engineering problems, it is generally perceived as a heuristic tool, without mathematical formalism and rigour. Recently, Rider *et al.* [14] demonstrated in a rigorous manner, the mathematical background of the volume tracking method which is often hidden by the geometrical manipulations involved. In fact, the volume tracking method is not limited to rectangular grids of finite differences. Conceptually, it can be applied to any type of mesh and implemented with most numerical schemes, such as finite elements and finite differences. An outline of the volume tracking method is given below to facilitate the understanding of its theoretical background. As one can see, no specific numerical scheme and mesh type is invoked in the demonstration.

For a given control volume i, which can be taken as a natural element resulting from a finite element discretisation, a piecewise constant value F_i is define to represent the filling state of element i

$$F_i = \frac{1}{V_i} \int_i f(\mathbf{x}, t)\, \mathrm{d}V_i, \tag{16}$$

where the limits of integration are restricted to the volume of an element V_i.

Therefore, the values of F_i, constant for each element, are referred to as the filling states of each element. According to this definition, the value of F_i (often called the 'filling factor') varies between 0 and 1. An element whose filling factor $F_i = 1$ is completely filled, while an empty element is represented by $F_i = 0$. A partially filled element has a filling factor between 0 and 1. The flow front is evidently contained within the partially filled elements.

Equation (15) is now integrated over the volume V_i,

$$V_i \frac{\partial F_i}{\partial t} + \int_{V_i} \mathbf{u} \cdot \nabla f \, \mathrm{d}V_i = 0. \tag{17}$$

Considering the continuity equation, $\nabla \cdot \mathbf{u} = 0$, Equation (17) can be written as

$$V_i \frac{\partial F_i}{\partial t} + \int_{V_i} \nabla \cdot (\mathbf{u} f)\, \mathrm{d}V_i = 0. \tag{18}$$

Discretising in time with finite differences, and applying the Gauss theorem transforms (18) into:

$$F_i^{n+1} = F_i^n - \frac{\Delta t}{V_i} \int_{\partial V_i} (\mathbf{u} f) \cdot \mathbf{n}_{\mathrm{ou}}\, \mathrm{d}S, \tag{19}$$

where F_i^{n+1} and F_i^n are the filling factors at time steps n and $n+1$, S is all surfaces of element i and n_{ou} is the outward unit normal.

The surface integral that appeared in (19) can be evaluated as a discrete sum of fluid quantity flowing in and exciting from all faces of element i

$$-\frac{\Delta t}{V_i} \int_{\partial V_i} (\mathbf{u} f) \cdot \mathbf{n}_{\mathrm{ou}}\, \mathrm{d}S = \frac{1}{V_i} \sum_j q_{ij} \Delta t; \quad q_{ij} = (\mathbf{u}_j \cdot \mathbf{n}_{\mathrm{in}})\, S_j, \tag{20}$$

where q_{ij} is the flow rate of fluid entering into element i across face j, and $\mathbf{u}_j$, $\mathbf{n}_{\mathrm{in}}$ and S_j are velocity vector, inward unit normal and area of face j respectively.

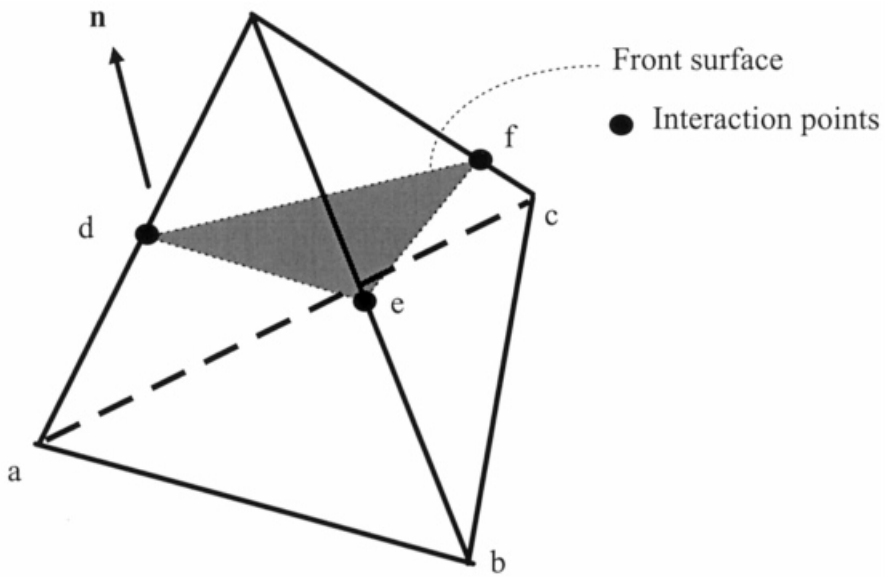

Figure 4. Scheme of calculation of the fluid quantity flowing into an element.

The volume tracking methods solves Equation (19) for each element instead of solving Equation (15) directly.

Since the tetrahedral elements are used for solving the Navier–Stokes equations in the present work, all implementation procedures for the volume tracking method are developed based on the same element topology.

In order to achieve a high precision of a volume tracking scheme, a reconstruction of the flow front interface contained by all interface elements, where $0 < F_i < 1$ is necessary to evaluate accurately its shapes and locations. The reconstruction includes the evaluation of the interface normal and the volume matching operation. The front interface within an element can be expressed mathematically by

$$\mathbf{x} \cdot \mathbf{n} = b, \tag{21}$$

where $\mathbf{x}$ represents any point on the interface, $\mathbf{n}$ is the unit normal of the interface and b is the interface constant.

The interface normal is calculated by

$$\mathbf{n} = \nabla f / |\nabla f| \quad \text{where } f \text{ is the filling factor.} \tag{22}$$

Since the filling factor is a piecewise content function, a least square procedure is implemented to calculate this vector.

Knowing the unit normal vector of the front interface and given a filling factor for an element, the exact position of the interface plan can be evaluated by matching the filled volume with the given filling factor. This volume matching involves some geometrical calculations, such as calculating the volume bounded by several polygon of three or four sides, and evaluation of the interaction points between the interface plane and the tetrahedral element. Figure 4 shows the case of tetrahedral element cut by the flow front surface. The filled portion is delimited by four faces (*abc*, *abed*, *cbef* and *acfd*) and the flow front surface (*def*). Once the front interface is reconstructed, the front advection can be realised by evaluating the flux

across all faces using expression (19). As the movement of the flow front is limited so as not to exceed more than one layer of elements within each time step, only elements near or across the flow front are used to evaluate the front movement.

In conclusion, the major contribution of this work is to combine a three-dimensional finite element scheme with a robust volume tracking technique. Instead of using rectangular grids as in conventional volume tracking techniques, the use of a tetrahedral mesh allows a much more flexible geometrical representation of the complex parts. The robustness of the volume tracking technique for unconstructured meshes is proved by all tests conducted and the combination of this technique with a FEM model provides an encouraging future for incorporate mesh adaptivity in order to increase the model precision with complex physical situations.

3.3. Coupling of the flow solution with front tracking

Another important aspect in solving the mould filling problems is the coupling between the flow solver and the front tracking operation. The flow solution is used to move the flow front, while the moving boundary delimits the flow domain, consequently affecting the flow solution. A proper choice of the time step is crucial to ensure an accurate solution within the constraints of the computation time. In most filling analysis, the flow front is subject to large distortions, separation, vortex formation, etc., and the geometry of the part can be very complex. Therefore, the concept of constant time step in classic CFD problems leads often to large variations of Courant number $Co = (u\Delta t)/h$ (also referred to as the CFL criterion) during a filling analysis. A small Courant number ($Co \ll 1$) will lead to a large computation time and become unusable for some complicated parts. On the other hand, using a large Courant number ($Co > 1$) causes the numerical scheme to become unstable and compromise the solution accuracy. A variable time step is preferable for most filling problems. The time step selection can be performed according to:

$$\Delta t = Co\ \mathrm{Min}(h_i/u_i); \quad i = 1, \text{ number of elements across or connected to the front,} \tag{23}$$

where h_i is the characteristic length of an element and u_i is the velocity magnitude in the same element.

Based on experience, a Courant number of 0.5 is recommended in the current study.

For every time step, a solution of the Navier–Stokes equations is performed with a Newton-type iteration in order to obtain the velocity distribution in the filled domain. Based on the velocity field, the fill factor of each element can be evaluated by expression (19). Finally, a newly filled domain is defined using the updated fill factor field with a reconstruction of the flow front. An iterative procedure is performed up to the end of the filling phase.

4. EXAMPLES AND DISCUSSION

As the filling problems involve the coupling of the flow equations and moving flow fronts, it is very difficult to establish benchmark tests to validate the entire numerical model. Several researchers have performed experimental set-ups, trying to obtain true data to compare with the numerical predictions [8,31,32]. The difficulties of using these experiments come from the lack of repeatability of the data and accurate control of the operating conditions. The alternative to this is to use a given velocity field, from which an analytical solution can be derived for the flow front position. In the following section, a 2D analytical test is presented

for validating the front tracking model. Other examples are presented to validate the entire numerical model and demonstrate its capabilities.

4.1. Analytical case

The example is a unit square where a velocity field is imposed as:

$$u = -y,$$
$$v = -x, \tag{24}$$

Since the velocity (24) is steady, the particle pathlines and the streamlines are coincident, and governed by

$$y^2 = x^2 + c, \tag{25}$$

where c is a constant.

The magnitude of the velocity vector $|U|$ is equal to $(x^2 + y^2)^{1/2}$. The initial front is assumed as straight lines $\underline{ab}$ and $\underline{bc}$ (see Figure 5). As the fluid fills the square cavity from the top and right sides, the velocity is diminishing and vanishes at the origin $\underline{o}$. Since the particle at the point $\underline{b}$ will flow along the square diagonal according to (25), the analytical solution of the non-dimensional displacement (d/D) versus filling time can be obtained:

$$d/D = 1 - e^{-t}, \tag{26}$$

where d is the particle displacement $|\underline{bb'}|$ and D is the length of the diagonal $|\underline{bo}|$ (see Figure 5).

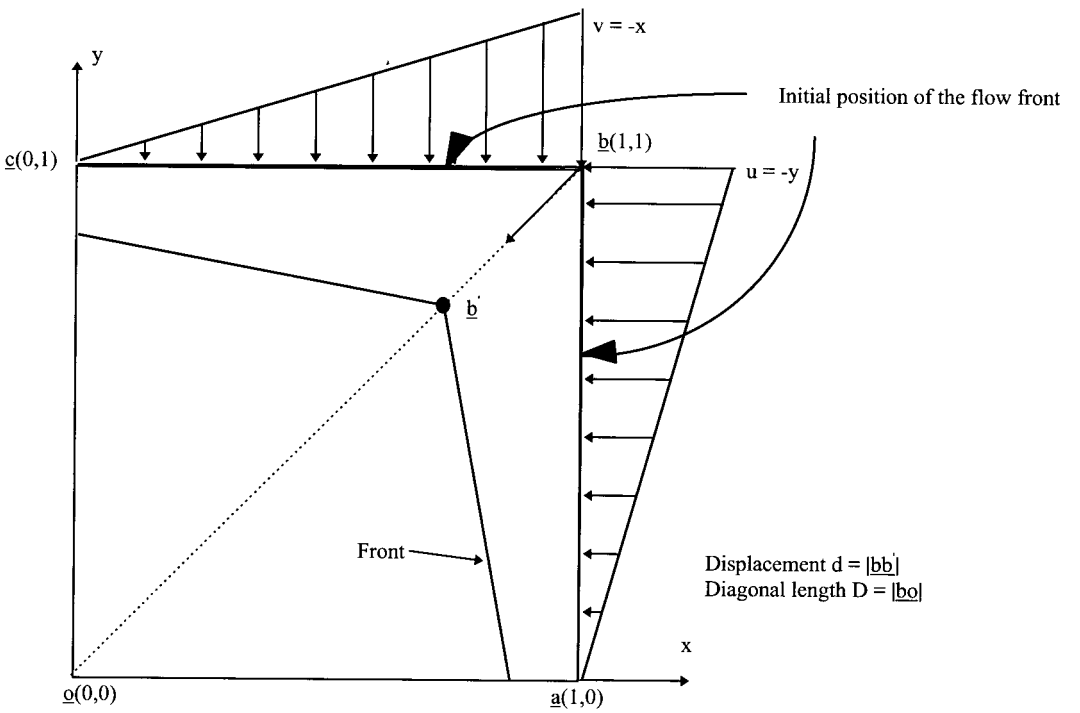

Figure 5. Validation test with a given velocity field.

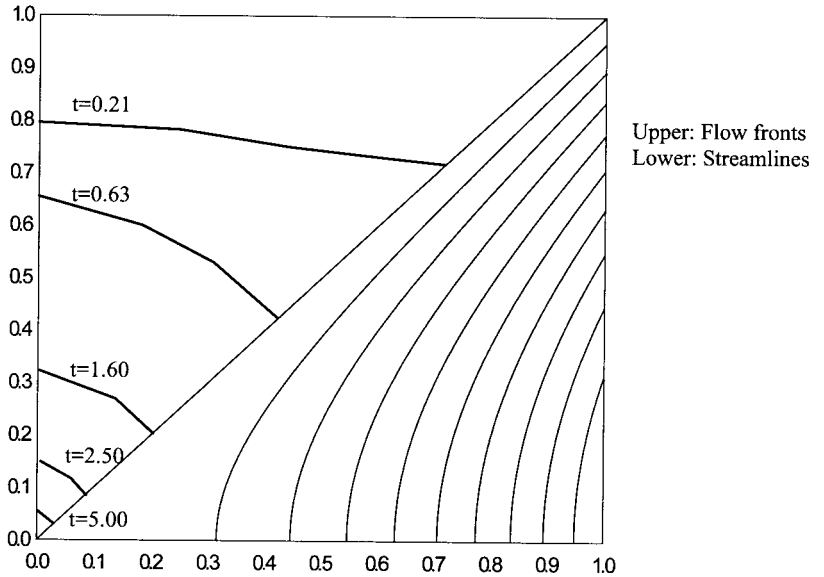

Figure 6. Plotted flow front positions (above the diagonal) and streamlines (below the diagonal).

The numerical flow fronts and the streamlines that are coincident with the particle pathlines are plotted in Figure 6. As expected, the front advancement along the diagonal is slowed down due to the imposed velocity.

In order to compare with the analytical solution, the flow front position at the diagonal is collected at various times. A very good agreement between the numerical prediction and analytical solution is obtained during the entire filling process (see Figure 7).

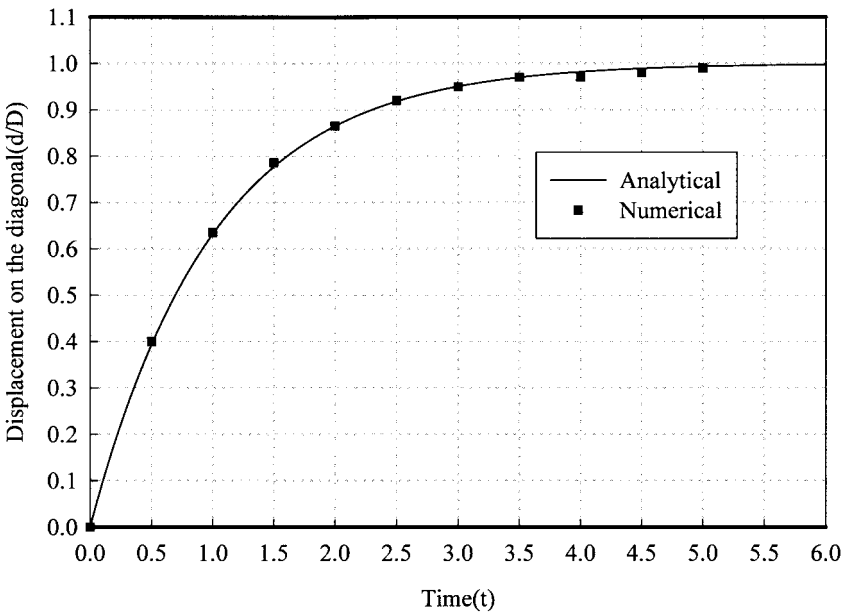

Figure 7. Comparison of the numerical prediction with the analytical solution.

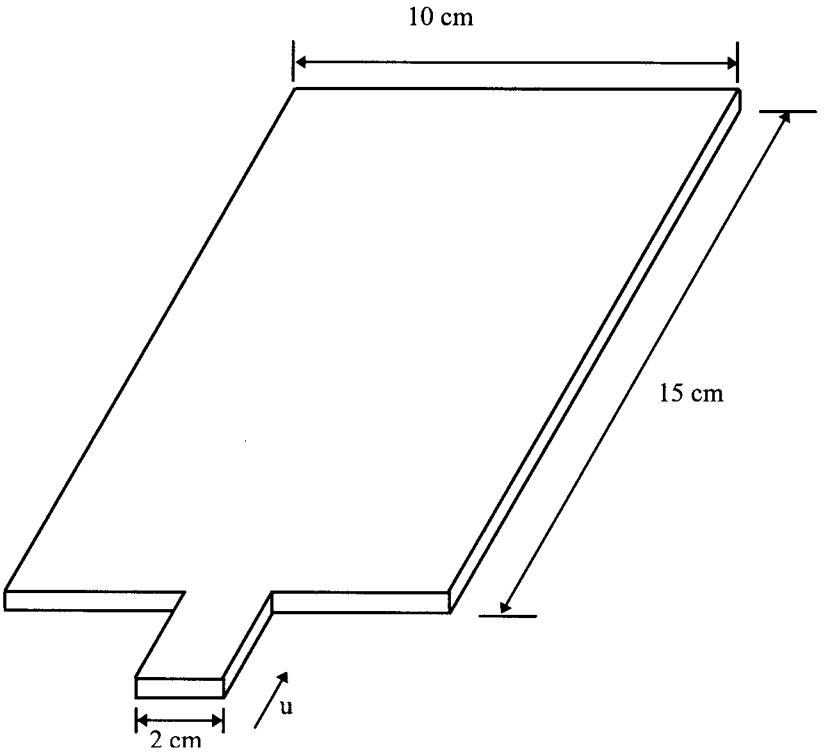

Figure 8. Geometry of the rectangular plate.

4.2. Filling of a rectangular plate

The filing of a three-dimensional rectangular plate of dimension 10 cm (width) $\times$ 15 cm (length) $\times$ 0.2 cm (height) is simulated. The plate has a narrow inlet of 2 cm width, which creates a sudden expansion when the liquid flows from the gate to the cavity (see Figure 8). The main objective of this example is to illustrate the inertia effect on the filling behaviour when the liquid is injected at high speed.

Since the rectangular plate is placed horizontally, the gravity term is neglected. The inlet velocity is uniform with a magnitude of 1 m s^{-1}. The friction boundary condition is imposed. Two different cinematic viscosities 0.1, 0.00001 $m^2 s^{-1}$ are simulated. The corresponding Reynolds numbers are 0.2, 2000 respectively, based on the entrance width. The figures in Plate 1 show the flow front positions for both cases at different filling stages. The red represents the filled area. Figures on the first row correspond to the viscous case ($Re = 0.2$), where the viscous force is dominant over the flow momentum. The fluids fills into the large cavity and expands uniformly in all directions. The predicted filling patterns change from a circle line to a straight one at the end. This type of filling behaviour is similar to that encountered in injection moulding of plastics and is well-verified by experiments. For the second case, when the liquid enters into the cavity, the flow is subjected to a sudden expansion. Since the inertia is dominant over the viscous forces and no vorticity is generated in the flow, the fluid behaves as 'rigid body', without spreading until it hits the wall at the top. After the jet hits the top of the cavity, the main flow stream is split into two symmetrical branches from the 'stagnation point' (see Plate 1). These streams turn back and join the main flow at the bottom of the cavity. Two air

pockets are formed at the end. The second and third rows represent the flow front positions and corresponding velocity vectors for the inertia case ($Re = 2000$). The inertia effect is clearly shown through this simulation. Finally, the critical areas for air entrapment are successfully predicted ('holes' formed at the end of the filling).

4.3. Filling of a step cavity

A 3D cavity is simulated to illustrate the gravity effects as well as the influence of the inertia. The geometry and the dimensions are shown in Figure 9. This example was first suggested by Gao *et al.* [3,4] to study the coupling effects of the inertia and gravity on the flow front movements. The cavity is fed by a fluid under a uniform velocity of 1 $m\,s^{-1}$. A friction boundary condition is applied at all surfaces of the mould. The kinematic viscosity used in this example is set to 0.0001 $m^2\,s^{-1}$, which leads to a Reynolds number of 300. To evaluate the gravity effects for a free-surface flow, the Froude number (Fr) is generally used as a characteristic number to represent the ratio between the inertia and the gravity forces. In this simulation, $Fr = 1.84$. This indicates that the gravity and inertia forces are at the same order and the flow will be affected by both forces. The numerical results are shown only on the middle plane (x–y) for the sake of display.

The flow front positions and the velocity fields are represented in Plate 2 at different filling times. The filling time (t/T) indicated below each pair of figures in Plate 2 is the ratio of the filling time (t) over the total filling time (T). Under such a definition, $t/T = 0$ represents the initial filling state and $t/T = 1.0$, the complete filling state. Figure 10 shows the maximum velocity as a function of the filling time. The velocity shown is non-dimensional, scaled by dividing the velocity over the inlet velocity. At the beginning of the filling stage, the flow accelerates and 'falls' towards the bottom under the effects of the gravity. The maximum velocity increases up to the three times as big as the inlet velocity (see Figure 10 at point 2 and Plate 2 at $t/T = 0.33$). When the flow hits the lower step, the flow is slowed down and the maximum velocity is consequently reduced (see points 3 and 4). After the collision with the lower step, the flow rises as a jet due to the dominant inertia effects. The flow is then decelerated by gravity acting in the opposite direction. The maximum velocity is reduced to 1.97 at $t/T = 0.50$. The gravity forces the main flow to stream preferably in the horizontal direction. After the flow meets the upper step of the cavity, a wavy front is generated as the

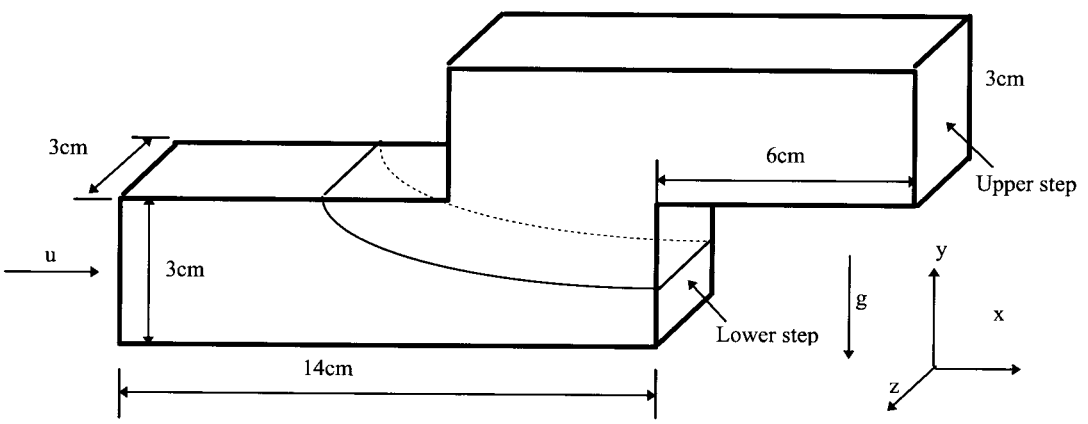

Figure 9. Geometry of the step cavity.

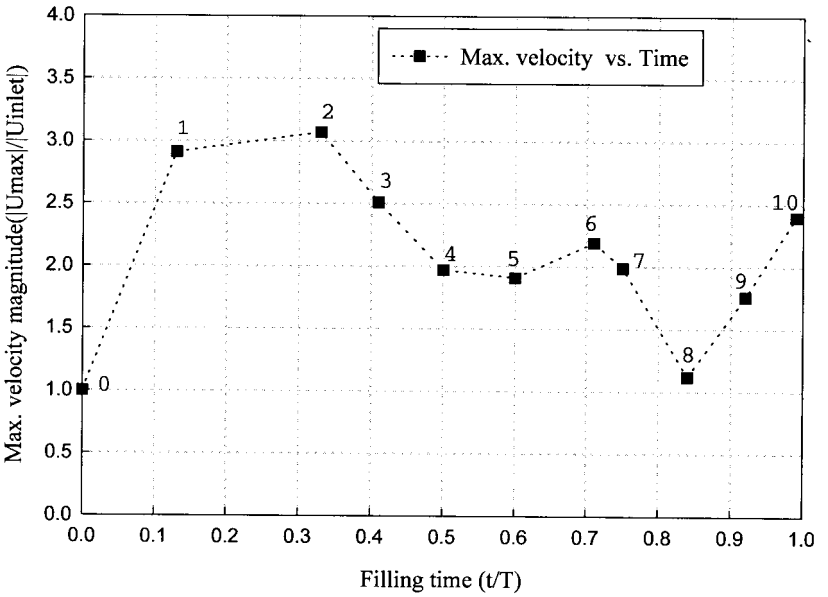

Figure 10. Plot of the maximum velocity at various filling time.

liquid flows back (at $t/T = 0.92$). Figure 10 shows clearly the flow's acceleration and deceleration caused by the coupling effects of the inertia and gravity during the filling process. Some characteristic points are shown in Figure 10:

- At $t/T = 0.33$ (point 2), the flow reaches its maximum velocity just before it encounters the lower step;
- From $t/T = 0.33$ to $t/T = 0.55$ (point 5), flow rising in the opposite direction of the gravity is decelerated;
- From $t/T = 0.71$ (point 6) to $t/T = 0.84$ (point 8), the flow is slowed down due to its collision with the upper step;
- In the last portion (from point 8 to point 10), the flow is accelerated until the complete filling.

4.4. Filling of a three-dimensional experimental part

In order to demonstrate the capabilities of the numerical prediction and validate the model in a realistic context, an experimental die casting part made with aluminium, is simulated. The part has a three-dimensional complex shape and the flow encounters large thickness variations (the thickness for runner, gate and cavity are 10, 1 and 2.3 mm respectively). Since the geometry is symmetrical (see Plate 3), only half the part is used for performing the calculations.

Table I. Material properties used in the simulations

Properties	Density (kg m^{-3})	Viscosity (Pa s)
Section 4.4: experimental part	2685.00	3.0×10^{-3}
Section 4.5: connector housing	2685.00	3.0×10^{-3}

The material properties are given in Table I. The part was meshed with 15735 tetrahedral elements. Since the viscous boundary layer is very thin compared with the mesh size, a slip boundary condition at the wall is assumed. The algebraic model described previously is used to calculate the eddy viscosity. The figures in Plate 3 show the filled portions and corresponding velocity magnitude at different filling stages. The shaded area in the figures on the left represent the portion filled by the fluid. Figures on the right show the velocity magnitudes as filling progresses. The red indicates the maximum velocity and the blue the minimum. As the runner is ten times thicker than the gate (10–1 mm), the liquid metal fills the runner first while a very small quantity flows into the front portion of the cavity. Once the runner is filled, the main flow stream starts filling the lateral part of the cavity due to the inertia effects. As the filling progresses, two flow streams meet each other at the centre, along the symmetry line. Two isolated holes are consequently created (see Plate 3). These isolated areas often entrap air and give rise the porosity in the final part. Another potential defect area is the 'ears' perpendicular to the top surface of the part. Due to the inertia, the liquid first fills the entire top surface before turning into the 'ears'. Therefore, such a numerical model can be used to predict the potential casting problems and help optimise the die and mould design.

4.5. Filling simulation of a connector housing

Filling analysis of an industrial part is performed using the current model. The part is a electrical connector housing made with aluminium 356. The material properties are shown in Table I. Since the part consists of two symmetrical connectors, only half of the geometry is meshed using tetrahedral elements. The mesh used for filling analysis contains 8299 nodes and 28736 elements. The eddy viscosity is calculated via the algebraic model. The figures in Plate 4 show the various filling stages and corresponding velocity magnitudes. The shaded area in figures on the left represent the portion filled by the fluid. Figures on the right show the velocity magnitudes as filling progresses. The red indicates the maximum velocity and the blue the minimum. Potential defect areas due to the multiple fronts merging are predicted, such as those indicated in Plate 4. The analysis provides detailed information on flow behaviour (maximum velocity, pressure requirement, etc.), which can be used to determine the proper dimensions of runners and gates, as well as the positions of the overflows.

5. CONCLUSION

A three-dimensional finite element model combined with a volume tracking method has been developed to simulate the cavity filling. A mixed formulation based on a four node tetrahedral element with a bubble function at the centroid ($P1^+/P1$) is employed and proved to be stable and effective in solving the flow with moving flow fronts. The volume tracking method developed in the frame work of three-dimensional unstructured meshes has shown its robustness for complex flow front motions. The combination of the FEM and volume tracking has been shown to be a very promising choice for handling mould filling problems. Examples have been presented to validate the numerical model and demonstrate its capabilities. Future work shall include the implementation of mesh adaptivity to improve interface reconstruction accuracy.

ACKNOWLEDGMENTS

The author would like to acknowledge the contribution of Mr Normand Nardini in meshing the experimental part and the connector presented in this paper.

REFERENCES

1. J.M. Floryan and H. Rasmussen, 'Numerical methods for viscous flows with moving boundaries', *Appl. Mech. Rev.*, **42**, 323–341 (1989).
2. K. Anzai and E. Niyama, 'Quasi-three-dimensional mold filling simulation system for prediction of defects in die-castings', *Modeling of Casting & Welding Processes IV*, TMS, Warrendale, PA, 1988, pp. 471–485.
3. D.M. Gao, G. Dhatt, J. Belanger and A. Ben Cheikh, 'A finite element simulation of metal flow in moulds', in R.W. Lewis and K. Morgan (eds.), *Numerical Methods in Thermal Problems*, Pineridge Press, Swansea, UK, 1989, pp. 421–430.
4. D.M. Gao, 'Modélisation numérique du remplissage des moules de fonderie par la méthode des elements finis', *Thèse de Doctorat*, Université de Technologie de Compiègne, 1991.
5. C.W. Hirt, 'A flow-3D study of the importance of fluid momentum in mold filling', in C. Kim and C.W. Kim (eds.), *Numerical Simulation of Casting Solidification in Automotive Applications*, TMS, Warrendale, PA, 1991, pp. 173–188.
6. W.S. Hwang and R.A. Stoehr, 'Computer aided fluid flow analysis of the filling of casting systems', *NUMI-FORM'86*, 1986, pp. 361–366.
7. R.W. Lewis, S. Usmani and J.T. Cross, 'Efficient mould filling simulation in castings by an explicit finite element method', *Int. J. Numer. Methods Fluids*, **20**, 493–506 (1995).
8. F. Mampaey and Z. Xu, 'Simulation and experimental validation of mould filling', *Modelling of Casting, Welding and Advanced Solidification Process VII*, TMS, Warrendale, PA, 1995, pp. 3–14.
9. D.M. St-John, K.G. Davis and J.G. Magny, 'Computer modelling and testing of metal flow in casting systems', *Can. Metall. Q.*, **20**, 359–368 (1981).
10. W.T. Sha, 'Fluid flow modeling in casting processes and its implications', *Modeling of Casting and Welding Processes IV*, TMS, Warrendale, PA, 1988, pp. 397–407.
11. H. Walther and P.R. Sahm, 'Simulating and modeling the filling of a mold', *Modeling of Casting and Welding Processes IV*, TMS, Warrendale, PA, 1988, pp. 635–644.
12. Y.F. Zhang, W.K. Liu and H.P. Wang, 'Cast filling simulations of thin-walled cavities', *Comput. Methods Appl. Mech. Eng.*, **128**, 199–230 (1995).
13. C.W. Hirt and B.D. Nichols, 'Volume of fluid (VOF) method for the dynamics of free boundaries', *J. Comp. Phys.*, **39**, 201–225 (1981).
14. W.A. Rider and D.B. Kothe, 'Reconstructing volume tracking', *Tech. Rep.*, *LA-UR-96-2475*, Los Alamos National Laboratory, 1997.
15. D.L. Youngs, 'Time-dependent multimaterial flow with large fluid distortion', in K.W. Morton and M.J. Baines (eds.), *Numerical Methods in Fluid Dynamics*, Academic Press, New York, 1982, pp. 273–285.
16. D.L. Youngs, 'An interface tracking method for a 3D Eulerian hydrodynamics code', *Tech. Rep.*, AWRE, 1984.
17. F. Mashayek and N. Ashgriz, 'A hybrid finite element–volume of fluid method for simulating free-surface flows and interfaces', *Int. J. Numer. Methods Fluids*, **20**, 1361–1380 (1995).
18. E. Thompson, 'Use of pseudo-concentration to follow creeping viscous flow during transient analysis', *Int. J. Numer. Methods Fluids*, **6**, 749–761 (1986).
19. J.F. Hétu, D.M. Gao, A. Garcia-Rejon and G. Salloum, '3D finite element method for the simulation of the filling stage in injection moulding', *Polym. Eng. Sci.*, **38**, 223–236 (1997) .
20. C.A. Hieber and S.F. Shen, 'A finite element/finite difference simulation of the injection molding filling process', *J. Non-Newtonian Fluid Mech.*, **7**, 1–32 (1980).
21. D. Gethin and S. Abdullah, 'Finite element formulation for filling a thin section cavity', *Int. J. Numer. Methods Heat Fluid Flow*, **7**, 344–366 (1997).
22. R. Mohammed, T. Osswald, T. Spiegelhoff and E. Sun, 'Modeling and simulation of high Reynolds number flows during reaction injection mold filling', *Int. Polym. Proc.*, **9**, 279–285 (1994).
23. S.P. Wang, 'Numerical simulation and experiment of incompressible viscous flow with moving free-surfaces', *Ph.D. Thesis*, Cornell University, 1993.
24. H. Schlichting, *Boundary-Layer Theory*, McGraw-Hill, New York, 1978.
25. B. Mohammedi and O. Pironneau, *Analysis of the k-ϵ Turbulence Model*, Wiley, New York, 1994.
26. Y. Shimomura, 'Subgrid-scale algebraic stress model of turbulence', *J. Phys. Soc. Jpn.*, **63**, 5–9 (1994).
27. J. Smagorinsky, 'General circulation experiments with the primitive equations', *Mon. Weather Rev.*, **91**, 99–164 (1963).
28. D.N. Arnold, F. Brezzi and M. Fortin, 'A stable finite element for the Stokes equation', *Calcolo*, **21**, 337–344 (1984).

29. C. Gay, P. Montmitonnet, T. Coupez and J.L. Chenot, 'Test of an element suitable for fully automatic remeshing in 3D elestoplastic simulation of cold-forging', *J. Mater. Process. Technol.*, **45**, 683–688 (1994).
30. R. Pierre, 'Optimal selection of the bubble function in the stabilization of the $P1-P1$ element for the Stokes problem', *SIAM J. Numer. Anal.*, **32**, 1210–1224 (1992).
31. M.C. Ashton and R.K. Buhr, 'Direct observation of the flow of molten steel in sand moulds', *Internal Rep.*, Department of Energy, Mines and Resources, Canada, 1973.
32. B. Sirrell, M. Holliday and J. Compbell, 'The benchmark test 1995', *Welding and Advanced Solidification Process VII*, TMS, Warrendale, PA, 1995, pp. 915–933.

